



## Evaluation of local soil-pile friction in saturated clays under cyclic loading

Rawaz Dlawar Muhammed, Jean Canou, Jean Claude Dupla, Alain Tabbagh

### ► To cite this version:

Rawaz Dlawar Muhammed, Jean Canou, Jean Claude Dupla, Alain Tabbagh. Evaluation of local soil-pile friction in saturated clays under cyclic loading. *Soils and Foundations*, 2018, 58 (6), pp.1299-1312. 10.1016/j.sandf.2018.06.006 . hal-01977778v2

**HAL Id: hal-01977778**

**<https://hal.science/hal-01977778v2>**

Submitted on 31 May 2021

**HAL** is a multi-disciplinary open access archive for the deposit and dissemination of scientific research documents, whether they are published or not. The documents may come from teaching and research institutions in France or abroad, or from public or private research centers.

L'archive ouverte pluridisciplinaire **HAL**, est destinée au dépôt et à la diffusion de documents scientifiques de niveau recherche, publiés ou non, émanant des établissements d'enseignement et de recherche français ou étrangers, des laboratoires publics ou privés.

## Evaluation of local soil-pile friction in saturated clays under cyclic loading

Rawaz Dlawar Muhammed, Jean Canou, Alain Tabbagh, Jean Claude Dupla

### ► To cite this version:

Rawaz Dlawar Muhammed, Jean Canou, Alain Tabbagh, Jean Claude Dupla. Evaluation of local soil-pile friction in saturated clays under cyclic loading. *Soils and Foundations, Japanese Geotechnical Society*, 2018, 58 (6), pp.1299-1312. 10.1016/j.sandf.2018.06.006 . hal-01977778

**HAL Id: hal-01977778**

**<https://hal.archives-ouvertes.fr/hal-01977778>**

Submitted on 7 Oct 2019

**HAL** is a multi-disciplinary open access archive for the deposit and dissemination of scientific research documents, whether they are published or not. The documents may come from teaching and research institutions in France or abroad, or from public or private research centers.

L'archive ouverte pluridisciplinaire **HAL**, est destinée au dépôt et à la diffusion de documents scientifiques de niveau recherche, publiés ou non, émanant des établissements d'enseignement et de recherche français ou étrangers, des laboratoires publics ou privés.

# **Local soil-pile friction evaluation in saturated clays under cyclic loading**

Rawaz Dlawar Muhammed<sup>1,2,3</sup>, Jean Canou<sup>1</sup>, Jean-Claude Dupla<sup>1</sup>, Alain Tabbagh<sup>2</sup>

<sup>1</sup> *Ecole des Ponts ParisTech, Navier laboratory, France*

<sup>2</sup> *Pierre and Marie Curie University, France*

<sup>3</sup> *Koya University, Iraq*

## **Corresponding Author:**

Rawaz Dlawar Muhammed

Ecole des Ponts – ParisTech, Navier laboratory

6 – 8 avenue Blaise Pascal, Cité Descartes, Champs-sur-Marne,

77455 Marne-La-Vallée, France

Phone : +33 1 64 15 35 46

Email: rawaz-dlawar.muhammed@enpc.fr

**ABSTRACT:**

The paper presents laboratory measurements of mobilized local friction along piles submitted to very large numbers of axial loading cycles. The experimental approach used is of the physical modelling type and consists in testing an instrumented prototype pile-probe installed and loaded in specimens of saturated clay reconstituted in a calibration chamber. The procedure developed for evaluating the local friction mobilized upon monotonic loading and further evolution during the application of displacement-controlled cycles, is described. After installation of the probe, a succession of monotonic and cyclic displacement-controlled loading phases, carried out on a reference kaolinite is presented and analysed. During the cyclic sequence, carried out up to  $10^5$  cycles, an initial phase of friction degradation is observed, followed by a reinforcement phase, which keeps going until the end of the test. A coefficient of evolution is defined allowing to quantify, during application of the cycles, the evolution of mobilized friction in terms of degradation or reinforcement of friction. The evolution of the friction mobilized during the application of the cycles is interpreted in terms of the combination of excess pore water pressure generation and dissipation. A comparison is made between maximum static shear mobilized before the cycles and after the cycles, showing the influence of the cyclic sequence on this quantity. Elements are finally given on the repeatability of the test, showing a fairly good level of repeatability.

**KEY WORDS:**

Pile, local shaft friction, cyclic loading, saturated clay, physical modelling, calibration chamber, instrumented pile-probe, excess pore water pressure

## 1 – INTRODUCTION

The study of the local friction behaviour of pile-soil interface constitutes an important issue in geotechnical engineering, related to the improvement of the design of foundations of railway bridges and offshore structures with an emphasis on wind turbines and oil and gas platforms. In particular, in the case of piles submitted to cyclic axial loadings due to environmental or industrial actions, this frictional behaviour is particularly complex and further experimental and theoretical research is still needed.

As far as experimental research is concerned, physical modelling approach based on calibration chamber testing appears to be a good way to better understand, under well-controlled laboratory conditions, the local behaviour of the soil-pile interface under cyclic axial loading.

Since the beginning of the years 80', experimental research has been developed on this subject, very often in relation with the offshore oil production industry and results have been presented, of the physical modelling approach type, using various types of probes representing sections of model piles, tested in soil specimens under various boundary and confinement conditions. Both sands and clays have been studied, most of the time for small to medium numbers of cycles, say less than  $10^4$  cycles.

As far as sands are concerned, one may cite the studies published by Chan and Hanna (1980), Lee and Poulos (1990), Al-Douri and Poulos (1995), Chin and Poulos (1996), Le Kouby et al. (2004), Lehane and White (2004), Tsuha et al. (2012). In most studies, the authors find a significant degradation of the mobilized friction during application of the cycles.

As far as clays are concerned, more specifically related to the subject of this paper, one may cite the results published by Poulos (1981a), Matlock et al. (1982), Goulois et al. (1985) or Procter and Khaffaf (1987). In particular, Poulos (1981a) conducted a number of small-scale laboratory tests on a model pile section (20 mm in diameter) in reconstituted saturated clay specimens (152 mm in diameter), up to maximum number of 1000 cycles, showing that two-

way displacement-controlled cycles cause significant reduction in pile-shaft skin friction which may result in failure of the model pile section. In particular, this author noted the strong influence of the amplitude of the cyclic displacement on the importance of the friction degradation.

Matlock et al. (1982) have conducted axial cyclic displacement-controlled load tests on a model pile section (2.5 cm in diameter) inserted into a confined reconstituted soft clay in a calibration chamber (76.2 cm diameter specimens). These authors have pointed out a significant reduction in mobilized friction during the application of the cycles (maximum number of 300 cycles applied).

As far as the behaviour of piles under very large numbers of cycles is concerned (several  $10^4$  to  $10^6$  cycles) corresponding to fatigue type of behaviour, it appears that very few if no publications are available. In the case of sands, Bekki et al. (2013) have presented results concerning the evolution of local friction along an instrumented pile-probe jacked into a sand specimen reconstituted in a calibration chamber, for large numbers of displacement-controlled cycles ( $10^5$  cycles). The results obtained show that after an initial degradation phase of the local skin friction (cyclic strain-softening), a reinforcement phase (cyclic strain-hardening) develops up to very high number of cycles ( $10^5$ ). However, for the case of fine-grained soils, typically saturated clays, no publication has been found on the subject in the literature.

Within this context, the objective of this paper is to present a complete laboratory prototype setup associated to a specific experimental procedure (physical modelling approach) which have been developed in order to study the local friction behaviour of soil-pile interface submitted to very large numbers of axial loading cycles, in the case of reconstituted saturated clay. After a description of the testing setup and of the experimental procedure developed, a typical test is presented and analysed, showing the interest of this prototype setup for better

understanding the mechanisms of local friction evolution along piles submitted to large to very large numbers of axial loading cycles.

## **2 – TESTING SETUP**

### **2.1 The calibration chamber testing setup**

The calibration chamber used in this research allows to reconstitute uniform soil specimens, 524 mm in diameter and 700 mm high. Independent vertical and horizontal stresses may be applied to the specimens, allowing to generate isotropic or anisotropic initial states of stress,  $K_0$  conditions, etc. The vertical stress is applied to the specimen through a large diameter bottom piston, the horizontal stress being applied through a water pressure confining the specimen contained in a neoprene membrane. Figure 1 presents a functional scheme of the calibration chamber showing the different parts of the setup. This calibration chamber is based on the same working principle as the ones described by Huang et al. (1988), Tumay and de Lima (1992) and Voyiadjis et al. (1993). The chamber itself is incorporated in a guiding and loading mechanical framework shown in figure 2. This framework allows the chamber to be moved and adjusted in translation and rotation on the rail track system, as shown in the figure. The four columns loading frame is equipped with two hydraulic jacks: a long stroke (1 m) 100 kN standard jack, allowing to perform displacement-controlled (0.1 to 100 mm/s adjustable displacement rate) push down operations, typically installation of probes, penetrometer testing, etc.; and a servocontrolled hydraulic actuator allowing to perform precise force or displacement-controlled loading operations, within the monotonic and cyclic ranges. Figure 3 presents a general view of the experimental setup.

This system has first been developed and used for sand testing, with development of a specific procedure for reconstitution of well-controlled sand specimens (dry and saturated) for carrying

out research on cyclic pressuremeter testing (Dupla and Canou 2003), on micropiles behaviour (Le Kouby et al. 2004) and on the behaviour of piles under cyclic loading (Bekki et al. 2013).

In order to study the behaviour of piles installed in saturated clay, complementary pieces of equipment as well as a specific experimental procedure have been recently developed and are presented in this paper. The main piece of equipment developed is a large size consolidometer described below.

## **2.2 New consolidometer developed for testing saturated fine-grained soils**

The consolidometer developed is a rigid wall reservoir composed of two adjustable halves (Plexiglas tube reinforced with metallic annular parts), equipped with a top and bottom draining plates, which allows to reconstitute 524 mm diameter and 600 to 800 mm high specimens of saturated clay under  $K_0$  conditions (no lateral deformation during the consolidation process) starting from a soil slurry. This reservoir is equipped with a loading frame and a double-action hydraulic jack which allows to consolidate the specimen by application of constant force increments to the top plate (Figure 4(a) and Figure 4(b)). The hydraulic jack is powered by a hydro-pneumatic pump which allows to apply controlled pressure steps to the jack and therefore controlled force increments. The jack piston is equipped with a force transducer and a long stroke “wire” displacement transducer which allow to monitor force and displacement during the consolidation process. Vertical as well as radial drainage circuits are available and may or may not be both activated during the consolidation process.

## **2.3 The instrumented pile-probe**

This prototype probe has been developed, within the framework of physical modelling research on piles, in order to make direct and independent measurements of tip resistance and local shaft friction representative of values occurring along a pile shaft. Figure 5 shows a simplified cross



section together with a view of the probe. The probe has a cross section of 10 cm<sup>2</sup> (diameter of 36 mm), similar to standard penetrometers. The conical tip is equipped with a 20 kN precision force transducer which measures the tip resistance upon loading. A friction sleeve is located on the shaft, far enough from the tip (240 mm above the tip), in order to minimize interactions between tip resistance and sleeve friction. The sleeve is 11 cm long (sleeve surface of 124.4 cm<sup>2</sup>) equipped with a  $\pm 5$  kN load sensor. The surface of the friction sleeve, as well as a significant part of the probe body, have been specially threaded in order to ensure a perfectly rough interface with respect to friction mobilization.

## **2.4 – Experimental procedure**

In order to prepare the initial clay slurry to be consolidated, dry clay powder is progressively added and thoroughly mixed with water, using a portable adjustable speed mixer, in order to prepare, in a large plastic container (200 l) a homogeneous clay slurry at a water content of about 1.5 times the liquid limit of the clay. This initial water content agrees fairly well with the recommendations suggested by Sheeran and Krizek (1971) as well as with the work of different authors (Anderson et al. 1991; Anderson et al. 2006; Cardoso and Nogueira 2013).

Once the preliminary mixing has been completed, the slurry is covered with a plastic film to prevent water from evaporating and left to soak for 48 hours to insure complete homogenization of the water content within the mixture. Finally, the slurry is mixed a second time for about 30 minutes in order to obtain a better homogenization.

The slurry is then poured from the preparation reservoir into the consolidometer using a long tube which avoids air entrapment into the slurry during the process (Figure 6 (a)). A thin layer of silicon grease has first been applied on the inner wall of the consolidometer with addition of a thin plastic film in order to minimize parasite side friction during the consolidation process and ease the “unmolding” process” of the specimen after transportation onto the calibration

chamber base. The loading frame is then adjusted and fixed on top of the consolidometer reservoir. The consolidation process is then initiated by applying successive increasing load increments up to the maximum value selected (Figure 6 (b)). For each load increment applied, the consolidation process takes place and the next force increment is only applied when the major part of the primary consolidation has been obtained under the given load.

During the application of each load increment, the applied force and top plate displacement are monitored, which allows to obtain the consolidation curve in terms of settlement versus time. After the consolidation process has been completed, the loading frame is removed. The reservoir is transported and adjusted on the bottom piston of the calibration chamber with a travelling crane (Figure 6 (c)). The two parts of the consolidation reservoir are then untighten, separated and carefully removed, not to disturb the clay specimen (Figure 6 (d)). The top end plate is then adjusted on top of the specimen as well as the lateral confinement rubber membrane, using a specially designed PVC tube internally equipped with the membrane “stuck” against it and slowly lowered around the specimen (Figure 6 (e)).

The lateral confinement cell and the top cover of the calibration chamber are then adjusted and tightened. Then lateral and vertical chamber pressures are progressively increased in order to decrease the negative excess pore water pressures existing inside the specimen and finally retrieve the state of effective stress initially generated in the consolidometer, with no residual excess pore water pressure (Figure 6 (f)). This final state is obtained after full stabilization of the vertical piston of the calibration chamber base. The specimen of saturated clay is then ready for further use.

### **3 – DESCRIPTION AND ANALYSIS OF A TYPICAL TEST**

#### **3.1 - Material used**

This typical test, called Test 1, has been carried out on a specimen of pure saturated kaolinite. The reference clay used, called Speswhite, is an industrial clay, that has been chosen in France as a reference clay for physical modelling purposes in geotechnics (in particular centrifuge and calibration chamber testing). Some of the geotechnical properties of this clay, as determined by the authors, are given in table 1. The grain size distribution curve of the deflocculated Speswhite clay has been determined using the sedimentometry method. It is shown in Figure 7, together with the curve given by the supplier.

#### **3.2 Clay specimen characteristics**

For this test, the clay specimen has been consolidated in the calibration chamber to a final vertical effective stress  $\sigma'_{v0}$  of 125 kPa and a final effective horizontal stress  $\sigma'_{h0}$  of 72 kPa corresponding to an estimated value of  $K_0$  equal to 0.58. In the consolidometer, the initial consolidation of the specimen has been achieved in four steps, corresponding to successive vertical stresses of 5, 15, 45 and 125 kPa. Figure 8 shows the corresponding settlement and vertical deformation versus time curves corresponding to the four successive load increments applied. The permeability and consolidation coefficient of the clay under this state of stress have been determined based on oedometer tests, giving  $k = 2.10^{-9}$  m/s and  $c_v = 2.10^{-7}$  m<sup>2</sup>/s

#### **3.3 Installation of the pile-probe**

After final consolidation of the specimen in the chamber, the pile-probe was first installed into the clay using the displacement-controlled long stroke hydraulic jack which allows to push the probe at a constant displacement rate (Figure 6 (g)). This installation process is representative of full displacement piles. The displacement rate used in this test was 1 mm/s. The probe was

pushed into the clay specimen until the friction sleeve was vertically centred within the specimen, corresponding to a penetration length of 460 mm of the tip into the specimen. Figure 9 presents the penetration curves obtained in terms of tip resistance, local friction and total force applied on top of the probe versus tip penetration depth during the installation process. It must be noted here that during the installation process as well as all subsequent loading operations, the boundary drainage of the specimen remains open.

The tip resistance increases rapidly during the initial phase of the penetration process (Figure 9(a)), down to a penetration depth of about 100 mm where a plateau is reached (about 0.25 MPa), corresponding to steady state conditions, accounting for a fairly good uniformity of the clay specimen.

The local friction starts to be mobilized when the friction sleeve gets into the specimen (Figure 9(b)), for a penetration depth of about 250 mm of the tip. The friction then increases to progressively reach an almost stabilized value close to 10 kPa when the final tip penetration depth of 460 mm has been reached.

The total load measured on top of the probe is shown in figure 9(c). This curve accounts for the global mobilization of both tip resistance and friction along the probe shaft. The rapid initial mobilization of total load corresponds to the initial mobilization of the tip resistance. The following almost linear increase of the total load observed then corresponds to the progressive increase of friction surface of the probe getting into the clay specimen.

### **3.4 Initial monotonic or « static » loading of the probe**

After the installation process has been completed, the probe is left alone without further loading for about 12 hours. This excess pore pressure dissipation time has been evaluated based on publications related to piezocone testing (Almeida and Parry, 1985; Kurup et al., 1994). It is also possible to use a theoretical solution proposed by Parez and Fauriel (1988), considering

the horizontal permeability of Speswhite ( $k_h=10^{-9}$  m/s (Feddemma and Bredeveld (2010)) to evaluate an approximate value of  $t_{50}$  ( $t_{50}$  equals to about 1500 seconds). Therefore, one may consider that 12 hours is largely enough to allow for practically complete dissipation of excess pore water pressures generated around the probe during the installation phase. Then, two successive displacement-controlled quasi-static monotonic compression loadings are applied to the probe up to failure (4mm total vertical displacement corresponding to about 11% of the probe diameter) with the servohydraulic actuator (Figure 6 (h)). The first loading is performed at a displacement rate of 30  $\mu\text{m}/\text{min}$ , the second one being performed at a rate of 300  $\mu\text{m}/\text{min}$ , after waiting 2 hours after the first loading. Contrary to the installation phase, for subsequent static loadings, the pore water pressure variation is mainly restricted to the interface zone for which only a thin layer of soil around the probe is involved (only a few millimeters thickness) with high values of local hydraulic gradient. The dissipation time is then significantly lower (Potts and Martins (1982)). Therefore, a duration of 2 hours is estimated to be enough to practically obtain full dissipation of EPWP. After each displacement-controlled loading, force-controlled unloading is applied. This procedure allows to evaluate the effect of loading rate on the results obtained, in terms of the drainage conditions around the probe during loading.

Figure 10 shows the results obtained for the typical test presented.

In terms of tip resistance (Figure 10(a)), for the first static test (30  $\mu\text{m}/\text{min}$  displacement rate), after a rapid initial mobilization of tip resistance for small displacements, the tip resistance still progressively increases until an almost stable value is reached for the final 4mm vertical displacement. Concerning the second static test (300  $\mu\text{m}/\text{min}$  displacement rate), a stiffer initial mobilization of tip resistance is observed until a plateau is relatively rapidly reached. It is, though, interesting to observe that the final values of tip resistance reached in both tests, equal to about 0.45 MPa, are very close to each other. It is also interesting to note that this value is

higher than the value of 0.25 MPa reached upon the installation process, carried out at a much higher penetration rate (1 mm/s).

In terms of local friction mobilization (Figure 10(b)), the responses observed for the two loadings are very close to each other, with a very rapid mobilization of local friction, followed by a plateau equal to about 17 kPa obtained in both cases. The only difference concerns a peak followed by a slight strain softening, observed at a very small displacement for the second loading.

The results are also shown in terms of the total force measured on top of the probe during loading (Figure 10(c)), which accounts for the local measurements made in terms of tip resistance and local friction.

As a conclusion, it is interesting to note that the failure characteristics obtained in terms of local friction and tip resistance are very similar for the two pre-cyclic static tests and that the second loading is not significantly affected by the first one. Also, in terms of drainage conditions around the probe during loading, these conditions should be very similar for the two loadings (similar levels of excess pore water pressure reached) since the results are very close in terms of friction and tip resistance.

### **3.5 Cyclic loading phase**

In order to investigate the influence of large numbers of loading cycles on the mobilization of local friction and tip resistance, cyclic displacement-controlled loading tests have been carried out on the probe after the initial static loadings. The main parameters involved in this type of cyclic tests are the displacement amplitude (alternated or non-alternated signal), the signal shape, the frequency of the signal and the number of cycles. In the test presented below,  $10^5$  cycles have been applied with a cyclic displacement amplitude  $\rho_c$  equal to  $\pm 250 \mu\text{m}$  (alternated signal) and a frequency of 1 Hz. The shape of the signal is sinusoidal. The local

displacement amplitude is known to be one of the key factors controlling the evolution of interface behaviour and the experimental setup developed allows to precisely investigate the influence of this parameter on the behaviours observed.

Figure 11 shows the corresponding results. Figure 11(a) shows the loading signal applied in terms of probe head displacement versus number of cycles (the probe is considered to be perfectly rigid and the probe head displacement is assumed to be the same as the local displacement at the friction sleeve level).

Figure 11(c) shows the probe response in terms of local friction mobilized versus number of cycles. A clear degradation process is observed from the very first cycle, which keeps going for about 50 cycles, corresponding to cyclic strain-softening of the probe-soil interface. Then, a progressive re-increase of mobilized friction is observed (cyclic strain-hardening) and keeps going, on an average, up to the end of the cyclic sequence (cycle n°  $10^5$ ) with a slight “re-decrease” observed between cycles 300 and 900. The degradation phenomenon, as observed in the initial part of the cyclic sequence, has already been observed by different authors on both model tests and field tests (Chan and Hanna 1980; Poulos 1981b; Poulos 1982; Matlock et al. 1982), but the following cyclic strain-hardening phenomenon (friction reinforcement), has not, to our knowledge, been previously described for fine-grained soils. In the case of dry sand, a similar friction reinforcement has been described by Bekki et al. (2013) for large numbers of cycles ( $10^5$  cycles).

In terms of tip resistance (figure 11 (b)), a similar trend is observed as for the friction evolution, with a degradation up to about cycle n° 40, followed by a progressive reinforcement of the tip resistance mobilization until the end of the test. The total head load response, as measured on top of the probe, is shown in figure 11(d). The evolution observed for the total head load globally accounts for the evolutions of both local friction and tip resistance measured independently. Figure 12 shows typical loading cycles in terms of local friction versus local

displacement. Figure 12(a) shows cycles corresponding to the degradation phase. A substantial reduction is observed on the maximum and minimum friction mobilized on each cycle, which begins at cycle n° 1 and continues up to cycle n° 50. Upon push in phases, the maximum friction mobilized, which was 17 kPa on the first cycle, drops to 5 kPa on the 50<sup>th</sup> cycle. Upon pull out phases, the evolution is similar with a maximum value of about 17 kPa (absolute value) and a minimum value of about 6 kPa. Figure 12(b) shows typical cycles corresponding to the cyclic strain-hardening phase which develops from cycle n° 50 to the last cycle (end of the test). It may be noted that the maximum value of friction obtained, upon push in and pull out phases at the end of the test ( $\pm 12$  kPa) is still lower than the one reached on the first cycle.

### **3.6 Final phase of static loading**

After completion of the cyclic sequence, it is important to perform new static compression load tests in order to quantify the influence of the cycles on the static failure parameters, in terms of tip resistance and local friction. In a way similar to the two static load tests carried out before the cyclic sequence, two static compression tests have been performed after the cycles in order to evaluate the post-cyclic response of the model. For the test presented in this paper, the two final static tests were performed at the same displacement rate of 300  $\mu\text{m}/\text{min}$  up to failure (4 mm vertical displacement). The first post-cyclic static test was performed directly after the end of the cyclic sequence while the second one was performed after a resting period of 2 hours after the first static test allowing for full drainage of the soil around the probe.

Figure 13 presents the results obtained in terms of mobilization of local friction and tip resistance versus vertical displacement.

In terms of local friction (Figure 13(b)), a significant difference may be observed between the two loadings. For the first post-cyclic loading, a sharp peak of friction (of about 23 kPa) is obtained for a low displacement (about 800  $\mu\text{m}$ ), followed by a significant strain softening



which keeps going with progressive stabilization for large displacements at an ultimate value of about 14 kPa. For the second post-cyclic loading, no peak is observed and full mobilization of friction is obtained for a very small displacement (about 100  $\mu\text{m}$ ) followed by a remarkably constant friction plateau of about 11 kPa, which is maintained up to large displacements. This second post-cyclic loading response is qualitatively very similar to the initial static response observed before the cyclic sequence. It is also interesting to note that the ultimate value of friction obtained at large displacements is very similar for both post-cyclic static loadings, accounting for a good consistency between the two successive loadings.

The comparison between pre-cyclic and post-cyclic static loading response shows that the cyclic sequence induces a significant “reinforcing” effect on the static friction that can be mobilized after cycling, which appears to be significantly higher than the friction mobilized before cycling. Also, it is interesting to note that the “memory” of the interface, due to the cycles may be easily erased by a first loading to failure. In terms of tip resistance, less differences are observed between the two successive loadings. The second loading appears more regular than the first one, with a progressive stabilization at about 0.35 MPa. The first loading appears less regular on its initial part with, however, a stabilization at about the same value as for the second loading (0.35 MPa), which is consistent.

For both local friction and tip resistance, the characteristic shape of the curves observed between 50 and 300 microns upon the first post-cyclic static loading, showing an upward concavity. This concave shape is typical of undrained shear with generation of negative excess pore water pressure, as usually observed in the triaxial apparatus upon shear. The interpretation of the differences observed between the pre-cyclic and post-cyclic static load tests in terms of mobilization of local friction is based on the following “well-known” principles: upon monotonic undrained shear test (triaxial test or interface shear test), normally consolidated clay exhibits positive excess pore water pressures (EPWP), due to contractive behavior whereas

overconsolidated clay exhibits negative EPWP due to dilative behavior (analogy with loose and dense sand behavior). When applied to our case, these principles result in the following interpretation: After installation and EPWP dissipation, the clay in the interface is in a normally consolidated state ( $\sigma'_n$  has increased in the process). Upon static undrained loading, positive EPWP will therefore certainly be generated, resulting in the loading curve presented in figure 14 (2<sup>nd</sup> initial static test). This interpretation is in full agreement with the results published by Potts and Martins (1982). Then the cyclic sequence occurs, which results in an initial increase of EPWP followed by a progressive decrease due to EPWP dissipation (this aspect has been analysed in detail in part 4.2 of the paper). It is believed that after full dissipation, the cyclic shear should result in a strongly densified and overconsolidated state of the clay within the interface zone, which should therefore lead, upon subsequent undrained shear (1st post-cyclic static test) in the generation of negative EPWP. This generation of negative EPWP will strongly increase the local shear measured during loading (peak value of 23 kPa, before softening), due to an overall increase of  $\sigma'_n$ . This hypothesis, generation of negative EPWP, is in good agreement with the statement reported by Randolph (2003) and is confirmed by the very typical shape of the shear curve, showing an upward concavity, accounting for a strong strain-hardening, typical of undrained shear with development of negative EPWP in triaxial testing (Henkel (1956); Koutsoftas (1981); Hattab & Hicher (2004); Henni et al. (2012); Berre (2014)). The following rapid decrease of friction (post peak softening) is attributed to strain localization within the interface.

Figure 14 finally shows a comparison between the static tests carried out before and after the cyclic sequence, in terms of local friction, showing that the ultimate friction mobilized after the cyclic sequence remains lower, in terms of ultimate value, than the friction mobilized before the cyclic sequence (about 11 kPa instead of 17 kPa). This decrease in terms of ultimate value accounts for an overall weakening of the interface due to the cyclic sequence.

The second post-cyclic static test is consistent with the first one in the sense that the overconsolidation effect has been erased by the first post-cyclic loading and the shape of the shear curve looks very much like the pre-cyclic static test.

## 4 – ANALYSIS OF THE CYCLIC SEQUENCE

### 4.1 – Coefficient of friction evolution

In order to quantify the evolution of local friction mobilization during cyclic loading, a coefficient called coefficient of friction evolution  $C_{e,fs}$ , has been defined as follows :

$$(1) \quad C_{e,fs} = \frac{f_{s,max(i)} - f_{s,min(i)}}{f_{s,max(1)} - f_{s,min(1)}}$$

where  $f_{s,max(1)}$  and  $f_{s,max(i)}$  are the maximum skin friction measured on first cycle and cycle  $i$  respectively (push-in phases),  $f_{s,min(1)}$  and  $f_{s,min(i)}$  being the values of minimum skin friction measured on first cycle and on cycle  $i$  respectively (pull-out phases).

This coefficient allows to clearly visualize the evolution of local friction mobilization during the application of the cycles and to easily make a distinction between degradation phases, corresponding to a decrease of  $C_{e,fs}$  and reinforcement phases, corresponding to an increase of this coefficient, and to quantify the importance of the degradation or reinforcement with respect to the initial mobilization observed on the first cycle.

Figure 15 shows a plot of this coefficient versus number of cycles for the test presented above, which clearly accounts for the initial degradation phase observed up to cycle n° 50, followed by the reinforcement phase toward the end of the cyclic sequence (with a slight decrease between cycle 300 to cycle 900). The minimum value reached is about 0.32 which is a fairly low value corresponding to a significant degradation. It may also be noted that even if re-increasing, the maximum value of  $C_{e,fs}$  reached at the end of the test is about 0.68, still significantly lower than 1.

## 4.2 – Analysis of the friction behaviour observed during the cyclic sequence

The analysis of the friction behaviour observed during the application of the cycles may be done in terms of the evolution of the effective normal stress acting on the probe shaft,  $\sigma'_n$ , the local friction mobilized being equal to  $f_s = \sigma'_n \tan \delta_{mob}$ ,  $\delta_{mob}$  being the mobilized friction coefficient. The evolution of  $\sigma'_n$  is directly related to the evolution of the excess pore water pressure  $\Delta u_s$  around the friction sleeve: when  $\Delta u_s$  increases,  $\sigma'_n$  decreases, resulting in a decrease of mobilized friction ; when  $\Delta u_s$  decreases,  $\sigma'_n$  increases, which results in an increase of mobilized friction.

It is believed that, in this low permeability clay, and by analogy with undrained cyclic triaxial testing on clays, cyclic shear at 1 Hz frequency will result in the development of excess pore water pressure (EPWP) close to the soil-probe interface. In fact, an heterogeneous field of EPWP will be created of small thickness, resulting in high hydraulic gradients and initiation of EPWP dissipation. The problem is therefore coupled with superposition of EPWP generation and dissipation.

There is, indeed, a competition between the excess pore water pressure generation mechanism due to “undrained” cyclic deformation of the clay around the sleeve, and the pore pressure dissipation phenomenon which starts taking place from the very beginning of the cyclic sequence due to the radial hydraulic gradient created by the excess pore pressure field. During the initial phase of the sequence (small numbers of cycles), the generation mechanism should be predominant with respect to dissipation, which should result in a relatively rapid increase of the resulting excess pore pressure, a corresponding decrease in the normal effective stress and corresponding decrease of mobilized friction (cyclic strain-softening). Then, the dissipation process should become predominant, resulting in a progressive decrease of the EPWP, re-increase of  $\sigma'_n$  and corresponding re-increase of mobilized friction (cyclic strain-hardening).

This decrease of excess pore water pressure should slow down with the number of cycles, which would explain the shape of the  $C_{e,fs}$  versus  $N$  curve for large numbers of cycles, when the conditions become practically fully drained. Figure 16 presents a conceptual scheme illustrating the above point. It appears that for the coupled case (generation coupled to dissipation of excess pore water pressure), the excess pore water pressure around the sleeve will first increase and then decrease after passing through a maximum value. This conceptual scheme is consistent with results presented by Procter & Khaffaf (1987) showing this type of evolution of the excess pore water pressure around a model pile cyclically loaded in a specimen of clay. The study presented by these authors is very interesting, with objectives close to ours, the main idea being to evaluate the influence of EPWP generation around a model pile element on the mobilization of friction. Even if the testing setup is slightly different from ours, the testing conditions are similar, with clay characteristics similar to ours. The loading conditions are also similar (displacement-controlled loading with similar range of displacement amplitudes and frequencies) and their results should, at least qualitatively, match ours. Figure 17 shows the evolution of cyclic EPWP close to their model pile element during cyclic loading ( $\Delta U_1$ ), clearly showing an initial increase followed by a decrease after a certain number of cycles (13 in this case). It is believed that the point corresponding to the maximum of excess pore water pressure should correspond to the minimum of mobilized friction and minimum value of  $C_{e,fs}$ . It will be very interesting in the future to try to make direct measurements of the pore water pressure around the probe in order to further check this hypothesis. For the test presented, the maximum excess pore water pressure would therefore be obtained at cycle n° 50. The slight re-decrease phase observed between cycles 300 and 900, before final reinforcement could be due to excess pore water pressure redistribution between the tip and the sleeve of the probe.

### 4.3 - Repeatability of the cyclic sequence

In order to evaluate the repeatability of the test and, in particular, the repeatability of the cyclic sequence, two more tests (Test 2 and Test 3) with same testing conditions and parameters as the ones implemented for Test 1 have been carried out. Figure 18 shows a comparison of the results obtained in terms of friction evolution coefficient. It may be observed that the trends obtained are qualitatively and quantitatively fairly similar for the three tests, accounting for a good level of repeatability of the test in terms of friction evolution. It is interesting to note that the relative decrease of  $C_{efs}$  observable between about cycle n° 300 and cycle n°900 is obtained in the three tests. This relative decrease has been interpreted above in terms of excess pore water pressure redistribution between the tip and the sleeve of the probe but this will need further validation.

It must also be noted here that the repeatability of the specimen preparation has also been checked by measuring the water content of the reconstituted specimens at different points on a given specimen (9 points) and by comparing the values obtained for different specimens (test 1, test 2 and test 3 in table 2). For those three specimens, an average value of 49.6% was found for the water content with a standard deviation of  $\pm 0.9$  %, which accounts for a fairly good repeatability of reconstitution of the specimens of saturated clay.

## 5 – CONCLUSIONS

In this paper, based on an original testing setup associated to a specific experimental procedure, corresponding to a physical model type of approach, the response of a pile-probe, in terms of local friction and tip resistance evolution, submitted to large numbers of cycles in a saturated clay (fatigue type of problems), have been presented.

A series of monotonic and cyclic displacement-controlled loading phases, carried out on a reference kaolinite, called Speswhite, have been presented, with description of the successive

phases of the tests and corresponding results. This type of tests allow, in particular, to quantify the evolution of local friction mobilization during the cyclic sequence as a function of the cyclic displacement amplitude and to quantify the effect of the cyclic sequence on the maximum static friction that can be mobilized at failure after the cycles, with respect to the initial value (before the cycles).

As far as the cyclic loading sequence is concerned, the test presented shows, after an initial phase of local friction degradation (cyclic strain-softening), a phase of friction reinforcement (cyclic strain-hardening) which keeps going up to very large numbers of cycles. The coefficient of friction evolution  $C_{e,fs}$  introduced allows to quantify the evolution of friction mobilization during the cycles, showing that even if this coefficient re-increase after an initial phase of decrease, its value remains below one (maximum value reached of about 0.70 for large numbers of cycles). As far as the static maximum friction is concerned, the application of the cycles results, with respect to the value obtained before the cycles, in a significant increase of static friction (peak value), however followed by rapid strain-softening.

Also, repeatability tests have been carried out, accounting for a good level of repeatability of the results obtained, thus validating the testing setup and the experimental procedure developed. Finally, this testing setup associated with the experimental procedure developed should help to better understand the behaviour of piles submitted to large numbers of axial loading cycles and therefore help to improve the design of such piles.

## ACKNOWLEDGEMENTS

The authors gratefully acknowledge the partial financial support by the SOLCYP project (2009-2015), a french national research project devoted to the improvement of the design of piles submitted to cyclic axial and lateral loads.

## REFERENCES

- Al-Douri, R. H. and Poulos, H.G., 1995. Predicted and Observed Cyclic Performance of Piles in calcareous sand. *Journal of Geotechnical Engineering ASCE* 121 (1): 1-16.
- Almeida, M. S, S. and Parry, R. H. G., 1985. "Small Cone Penetrometer Tests and Piezocone Tests in Laboratory Consolidated Clays," *Geotechnical Testing Journal*, GTJODJ, Vol. 8, No. 1, March, pp. 14-24.
- Anderson, W. F., Nguyen, D. H. and Adrian, F. L. 2006. A New Analysis Of Data From Statnamic Tests On Piles In Clay. In *Proceedings of the 10th International Conference On Piling And Deep Foundations*, Amsterdam, The Netherlands, pp. 618-626 .
- Anderson, W. F., Pyrah, I. C. and Fryer, S. J., 1991. A Clay Calibration Chamber for Testing Field Devices. *Geotechnical Testing Journal* 14(4): 440-450.
- Bekki, H., Canou, J., Tali, B., Dupla, J.-C. and Bouafia, A., 2013. Evolution of Local Friction Along a Model Pile Shaft in a Calibration Chamber for a Large Number of Loading Cycles. *Comptes Rendus - Mecanique* 341(6): 499-507.
- Berre, T., 2014. Effect of sample disturbance on triaxial and oedometer behaviour of a stiff and heavily overconsolidated clay. *Canadian Geotechnical Journal*, 51:896-910, <https://doi.org/10.1139/cgj-2013-0077>
- Cardoso, R. and Nogueira, J. S., 2013. An Experimental Study on the Consolidation of Soft Clayey Soils Using Electrochemical Methods. In *Proceedings of the 18th International Conference on Soil Mechanics and Geotechnical Engineering*. Paris, France, pp. 891-894.



511 Chan, S.F. and Hanna, T. H., 1980. Repeated Loading on Single Piles in Sand. Journal of  
512 Geotechnical Engineering 106(2): 171-188.

513 Chin, J. T. and Poulos, H. G., 1996. Tests on Model Jacked Piles in Calcareous Sand.  
514 Geotechnical Testing Journal 19(2): 164 180.

515 Dupla, J.-C., Canou, J., 2003. Cyclic pressuremeter loading and liquefaction properties of  
516 sands. Soils and Foundations 43(2): 17-31.

517 Feddema, A., Breedevelt, J. and Van Tol, A. F., 2010. Lateral loading of pile foundations due  
518 to embankment construction. Numerical Methods in Geotechnical Engineering: 631–636

519 Goulois, A., Whitman, R. V. and Høeg, K., 1985. Effects of Sustained Shear Stresses on the  
520 Cyclic Degradation of Clay. Strength Testing of Marine Sediments: Laboratory and In-  
521 situ Measurements, ASTM STP 883, R. C. Chaney and K. R. Demars, Eds., American  
522 Society for testing and Materials, Philadelphia, pp. 336-351.

523 Hattab, M. and Hicher, P. Y., 2004. Dilating behavior of overconsolidated clay. Soils and  
524 Foundations, Japanese Geotechnical Society, 2004, 44 (4), pp.27-40.  
525 <10.3208/sandf.44.4\_27>.

526 Henkel, D. J., 1956. The effect of overconsolidation on the behaviour of clays during shear.  
527 Geotechnique, 6, 139-150

528 Henni, A. D., Arab, A., Khelafi, H., 2012. Laboratory study of overconsolidated ratio of the  
529 undrained soil behavior. *2nd International Seminar INVACO – Innovation & Valorization*  
530 *in Civil Engineering & Construction Materials*

531 Huang, A.-B., Holtz, R. D. and Chameau, J.-L., 1988. A Calibration Chamber for Cohesive  
532 Soils. *Geotechnical Testing Journal* 11(1): 30-35.

533 Koutsoftas, D. C., 1981. Undrained Shear Behavior of a Marine Clay. *Laboratory Shear*  
534 *Strength of Soil*. ASTM STP 740. R. N. Yong and F. C. Townsend, Eds., American  
535 Society for Testing and Materials, 1981, pp. 254-276.

536 Kurup, P. U., Voyiadjis, G. Z. and Tumay, M .T., 1994. "Calibration Chamber Studies of  
537 Piezocone Test in Cohesive Soils" *Journal of Geotechnical Engineering*, Vol. 120, No. 1,  
538 January, pp. 81-107.

539 Le Kouby, A., Canou, J. and Dupla, J.-C., 2004. Behaviour of Model Piles Subjected to Cyclic  
540 Axial Loading. In *Proceedings of the International Conference on Cyclic Behaviour of*  
541 *Soils and Liquefaction Phenomena*, Bochum, Germany, 31 March - 2 April 2004, pp.  
542 159-166.

543 Lee, C. Y. and Poulos, H. G., 1990. Experimental Investigations of Axial Capacity of Model  
544 Grouted Piles in Marine Calcareous Sediments. Research Report No. R618, University of  
545 Sydney, School of Civil and Mining Engineering.

546 Lehane, B. M. and White, D. J., 2004. Friction Fatigue on Displacement Piles in Sand.  
547 *Géotechnique* 54(10): 645-658.

548 Matlock, H. , Bogard, D. and Cheang, L. 1982. A Laboratory Study of Axially Loaded Piles  
549 and Pile Groups Including Pore Pressure Measurements. In *Proceeding of The Third*  
550 *International Conference on the Behavior of Offshore Structure (BOSS)*, Vol. 1, pp. 105-  
551 121.

552   Parez, I. and Fauriel, R., 1988. Le piézocône. Améliorations apportées à la reconnaissance de  
553       sols. *Revue Française de Géotechnique* 33: 13-27.

554   Potts, D. M. and Martins, J. P., 1982. The Shaft Resistance of Axially Loaded Piles in Clay.  
555       *Geotechnique*, Vol. 32, No. 4, pp. 369-386. Poulos, H. G., 1981a. Some Aspects of Skin  
556       Friction of Piles in Clay Under Cyclic Loading. *Geotechnical Engineering*, Vol. 12, No.  
557       1, pp. 1-17.

558   Poulos, H. G., 1981b. Cyclic Axial Response of Single Pile. *Journal of Geotechnical*  
559       *Engineering Division* 107(1): 41-58.

560   Poulos, H. G., 1982. Influence of Cyclic Loading on Axial Pile Response. R413 Monograph,  
561       University of Sydney, Sydney, New South Wales 2006 Australia, 36 p.

562   Procter, D. C. and Khaffaf, J. H., 1987. Cyclic axial displacement tests on model piles in clay.  
563       *Géotechnique* 37(4): 505-509.

564   Randolph, M. F., 2003. Science and empiricism in pile foundation design. *Geotechnique* 53,  
565       No. 10, 847–875

566   Sheeran, D. E. and Krizek, R. J., 1971. Preparation of Homogeneous Soil Samples by Slurry  
567       Consolidation. *Journal of Materials* 6(2): 356-373.

568   Tsuha, C. H. C., Foray, P. Y., Jardine, R. J., Yang, Z. X., Silva, M. and Rimoy, S., 2012.  
569       Behaviour of Displacement Piles in Sand Under Cyclic Axial Loading. *Soils Foundations*  
570       52(3): 393-410.

571   Tumay M. T. and De Lima, D. C., 1992. Calibration and Implementation of Miniature Electric  
572       Cone Penetrometer and Development, Fabrication and Verification of the LSU In-Situ

573        Testing Calibration Chamber (LSU/CALCHAS). FHWA Research Report No.GE-92/08,  
574        Louisiana Transportation Research Center, Baton Rouge, LA.

575    Voyiadjis, G. Z., Kurup, P. U. and Tumay, M. T., 1993. Preparation of Large-Size Cohesive  
576        Specimens for Calibration Chamber Testing. Geotechnical Testing Journal 16(3): 339-  
577        349.

# Local soil-pile friction evaluation in saturated clays under cyclic loading

## FIGURES

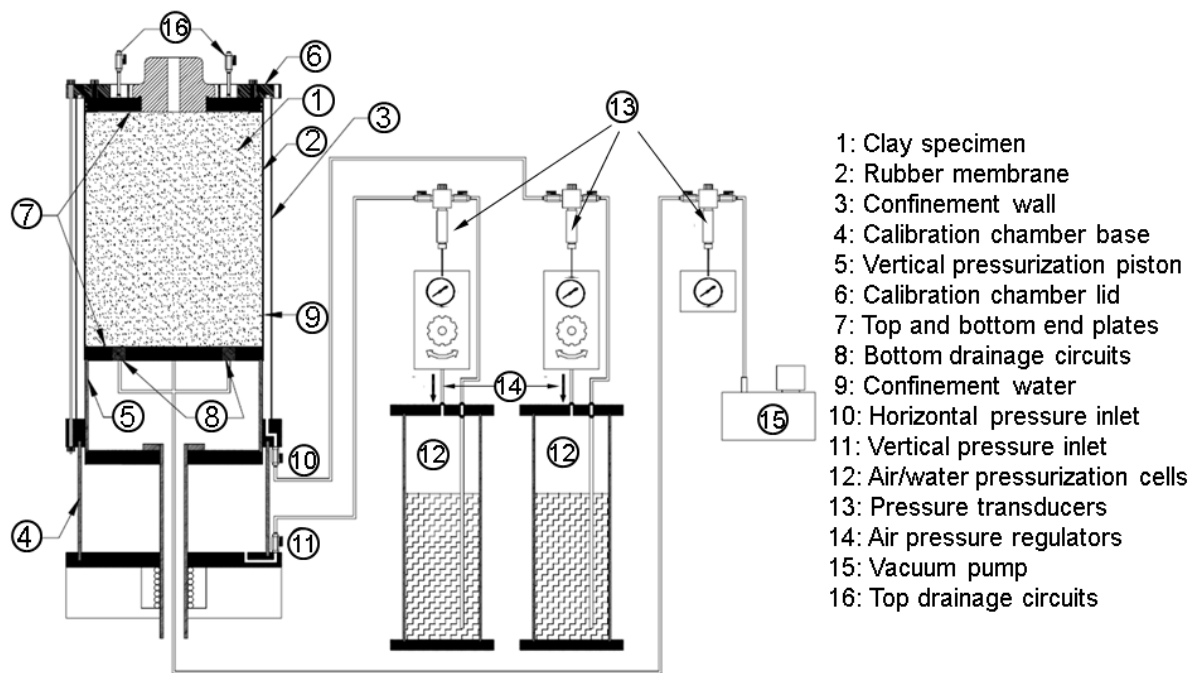


Fig. 1. Functional scheme of the calibration chamber setup

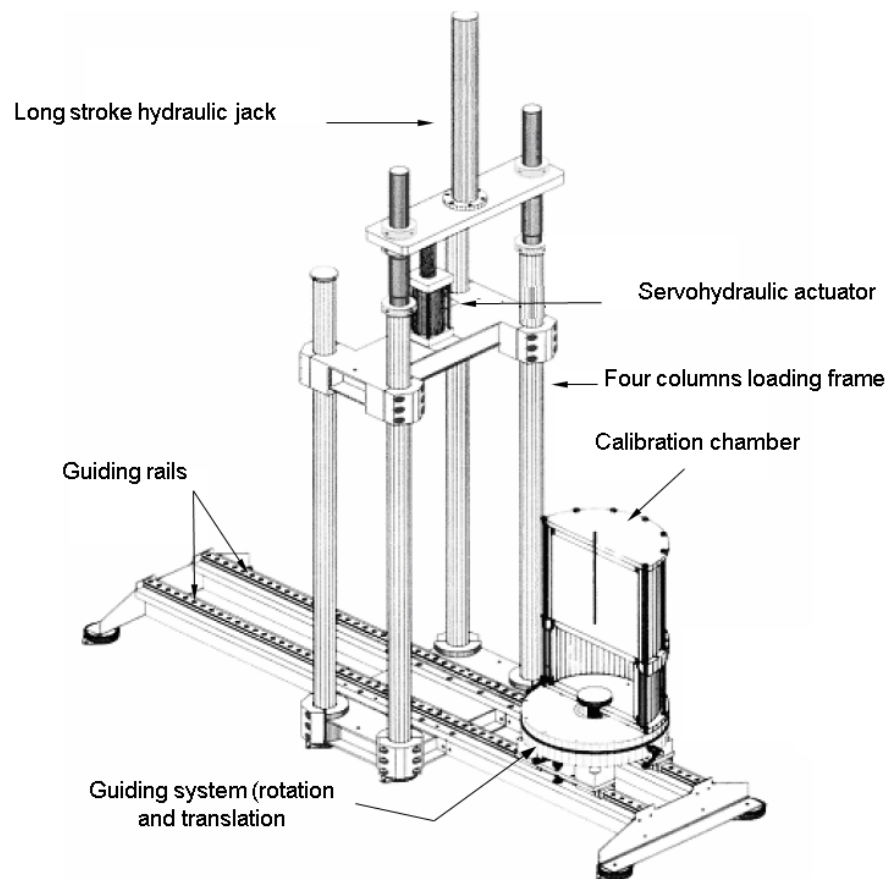
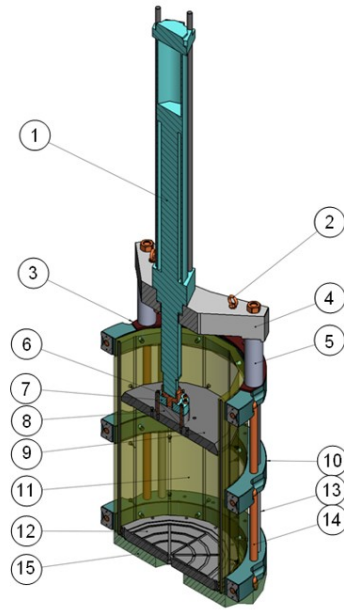


Fig. 2. Functional scheme of the complete setup, including guiding and loading framework

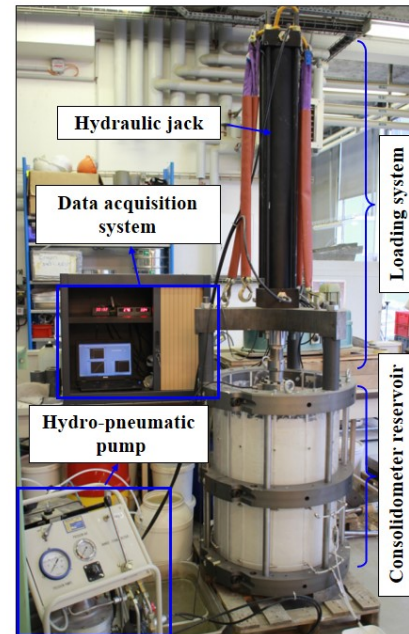


Fig. 3. Overall view of the experimental setup including the control and data acquisition booth

- 1 : Hydraulic jack
- 2 : Lifting rings
- 3 : Positioner
- 4 : Loading frame
- 5 : Loading columns
- 6 : Fitting piece
- 7 : Force transducer
- 8 : Protection piece
- 9 : Top loading and draining plate
- 10 : Metallic reinforcements
- 11 : Plexiglas tube with radial outward drainage
- 12 : Bottom draining plate
- 13 : Intermediate rods
- 14 : Metallic rods
- 15 : Base frame



(a)



(b)

Fig. 4. Consolidometer set up and ancillary equipment: (a) 3-D drawing showing one half of the consolidometer, (b) Overall view of the consolidometer set up and ancillary equipment



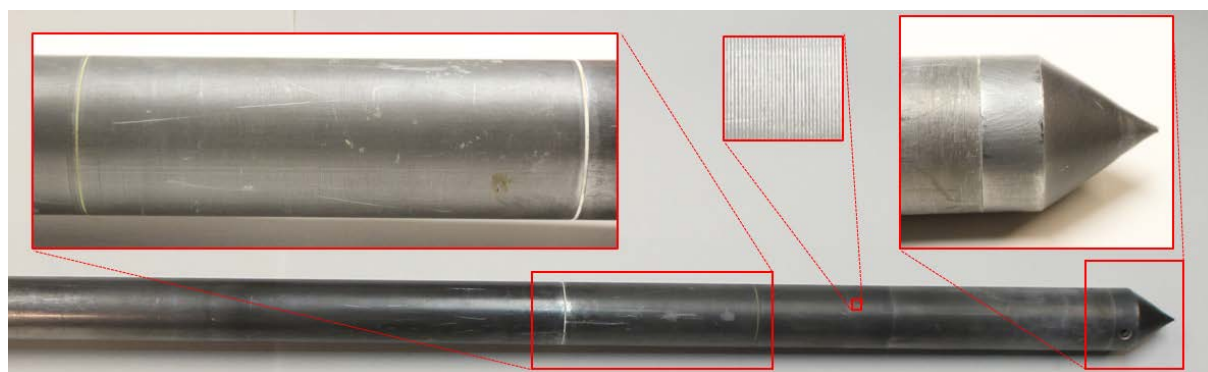
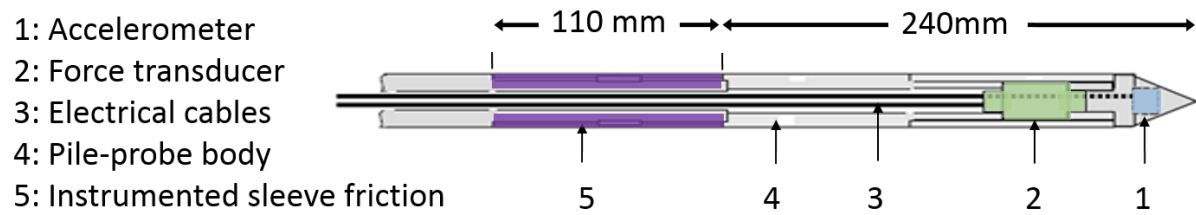


Fig. 5. Simplified cross-section and view of the instrumented pile-probe



(a)



(b)



(c)



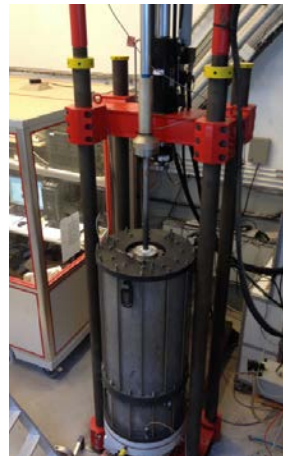
(d)



(e)



(f)



(g)



(h)

Fig. 6. Experimental procedure : (a) pouring the kaolinite slurry into the consolidometer, (b) application of increasing load increments (consolidation process), (c) adjustment of the clay specimen on the piston of the calibration chamber, (d) removing the consolidometer reservoir, (e) adjustment on top of the specimen the lateral confinement rubber membrane, (f) application of the initial state of stress to the specimen, (g) installation of the pile-probe, (h) ongoing test (after installation of the pile-probe)

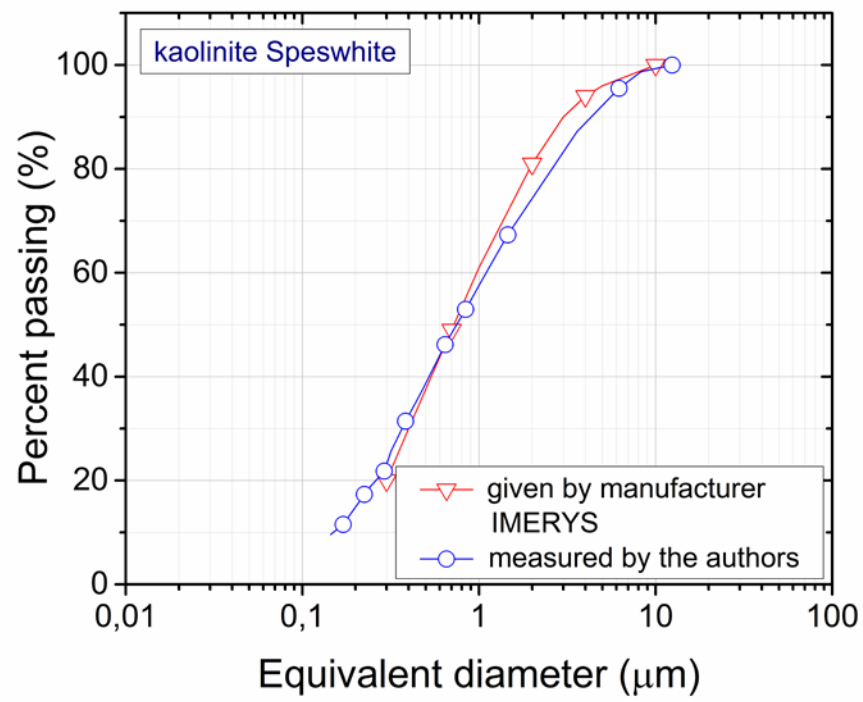


Fig. 7. Grain size distribution curves of Speswhite kaolinite

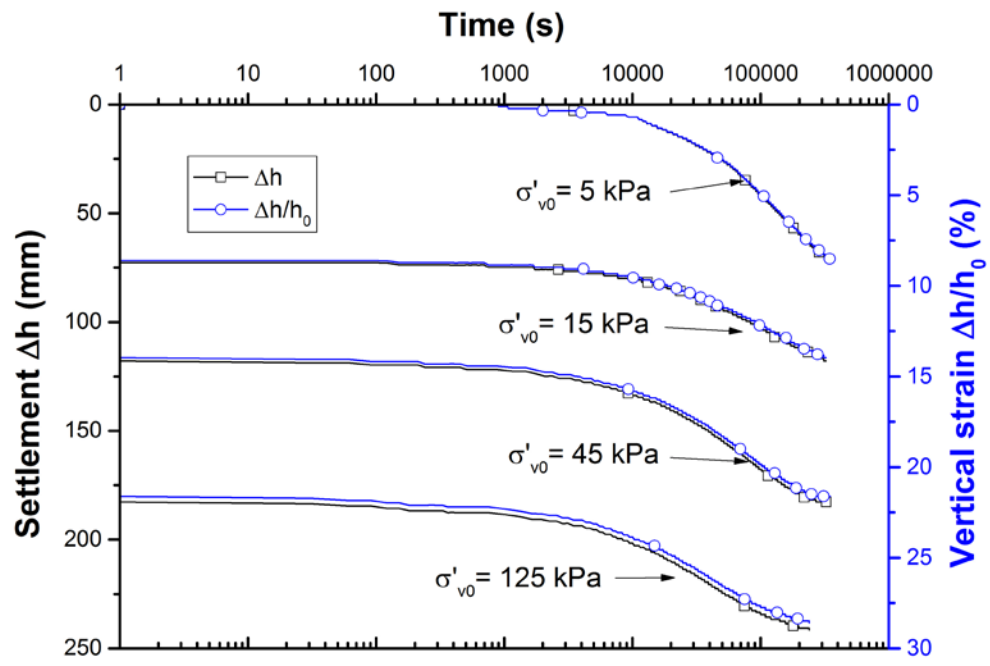
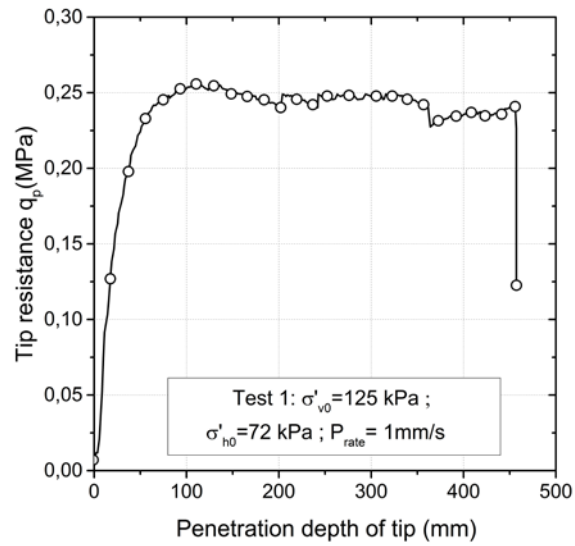
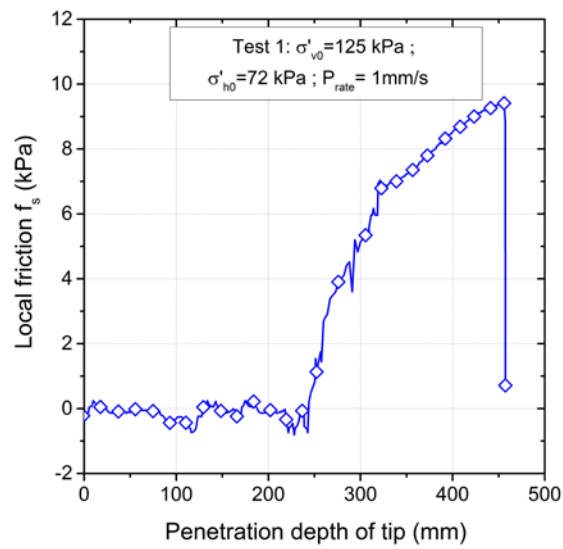


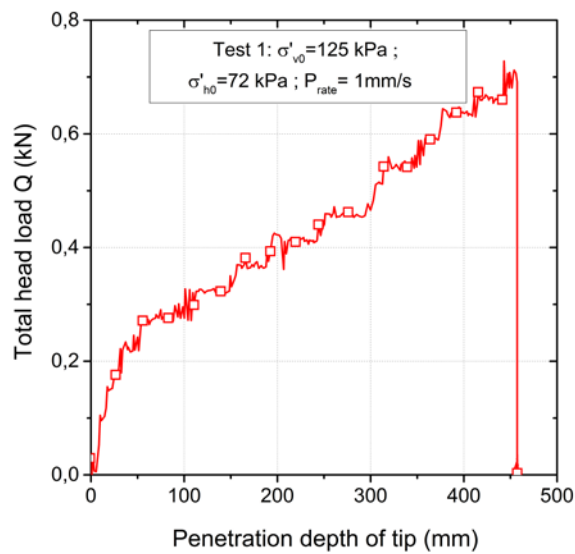
Fig. 8. Settlement and vertical strain versus time consolidation curves



(a)

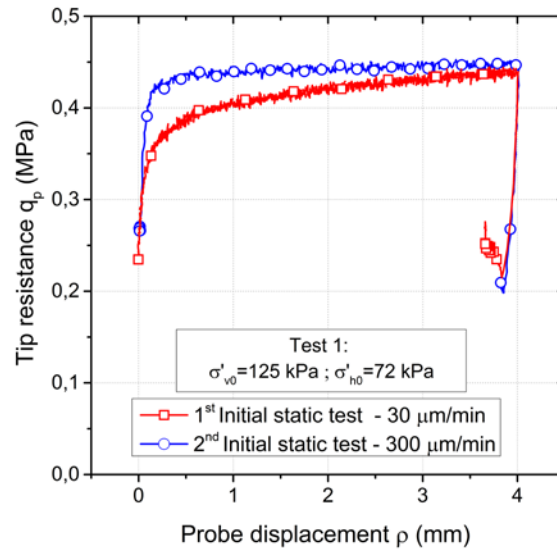


(b)

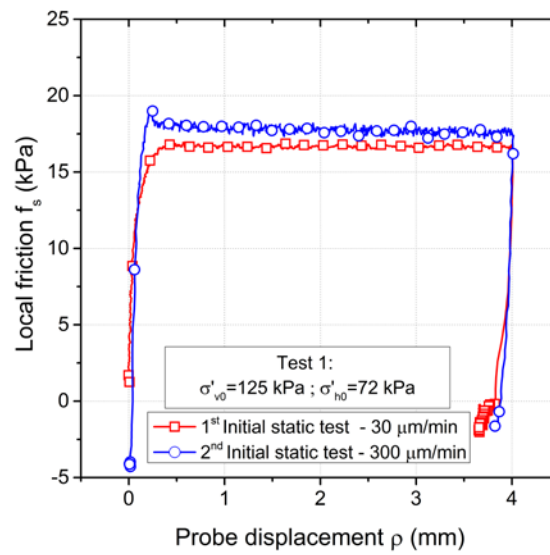


(c)

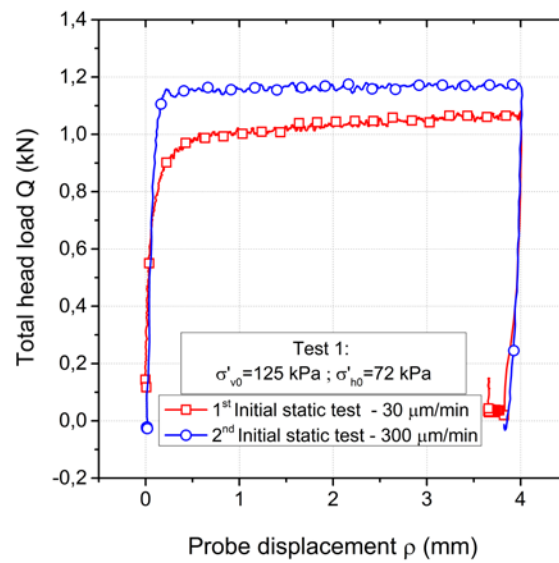
Fig. 9. Installation phase: (a) tip resistance versus penetration depth, (b) local friction versus penetration depth, (c) total load applied versus penetration depth



(a)

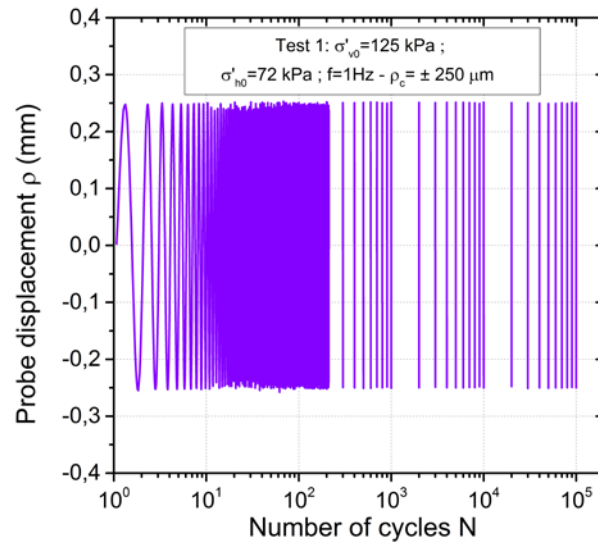


(b)

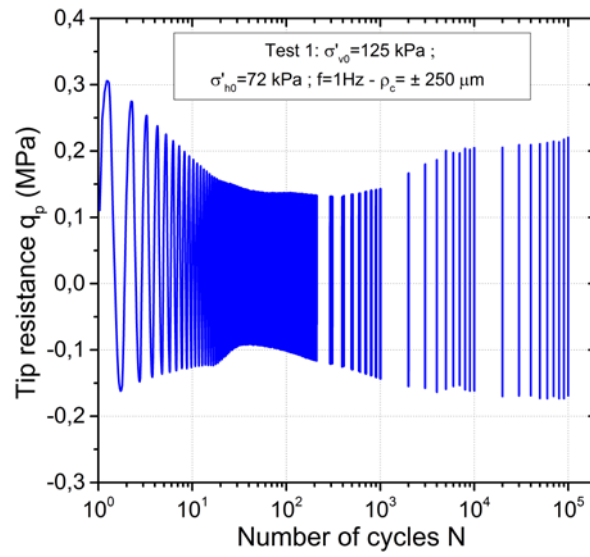


(c)

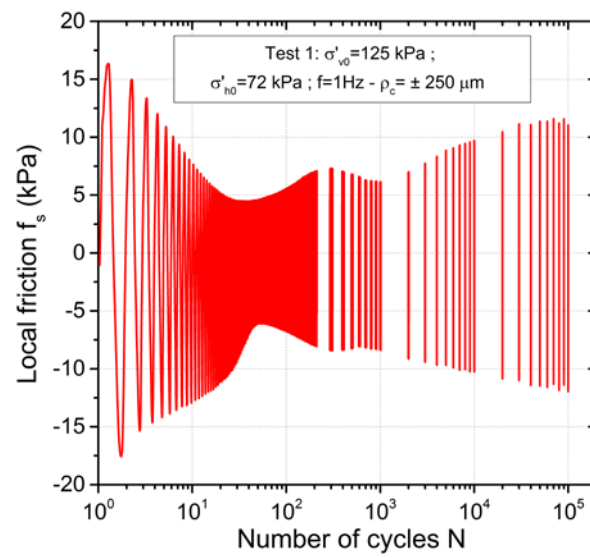
Fig. 10. Initial static loading tests: (a) tip resistance versus vertical displacement, (b) local friction versus vertical displacement, (c) total load applied versus vertical displacement



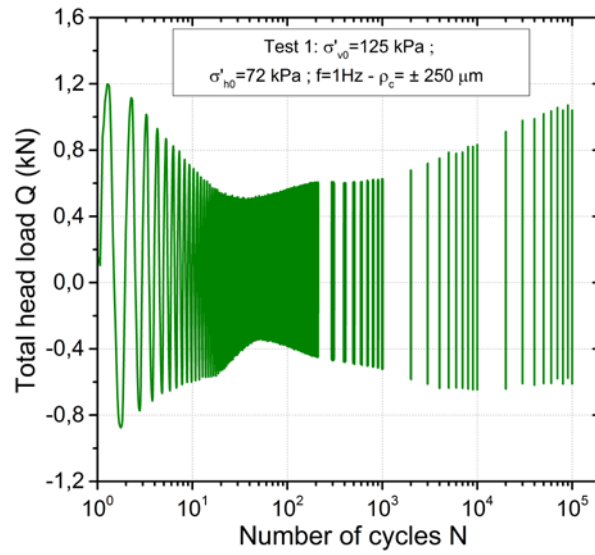
(a)



(b)



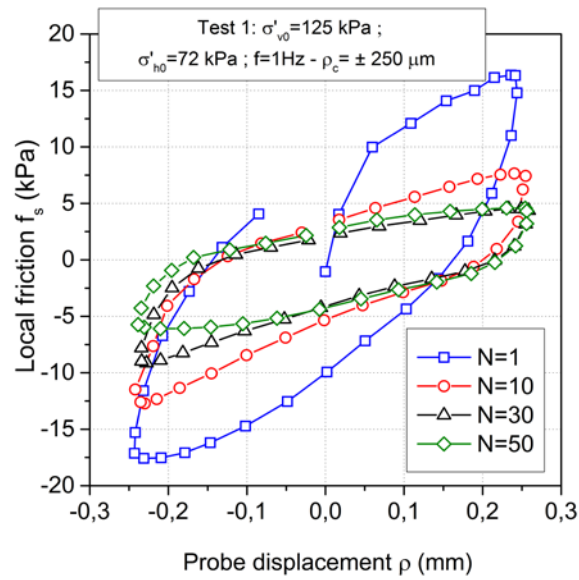
(c)



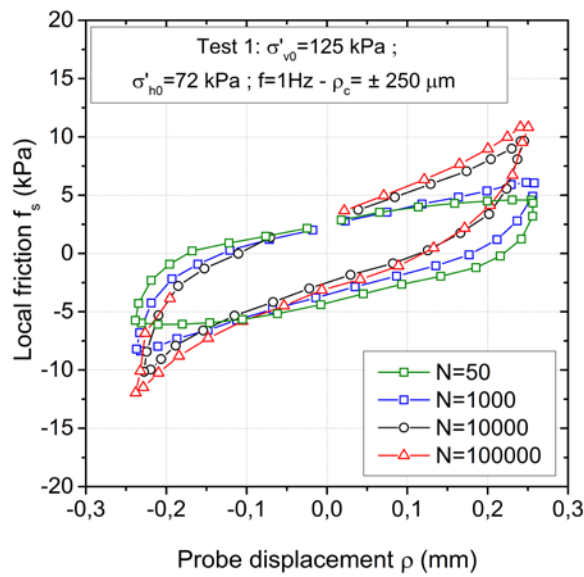
(d)

Fig. 11. Cyclic loading phase: (a) displacement-controlled loading signal versus number of cycles, (b) tip resistance versus number of cycles, (c) local friction versus number of cycles, (d) total load applied versus number of cycles



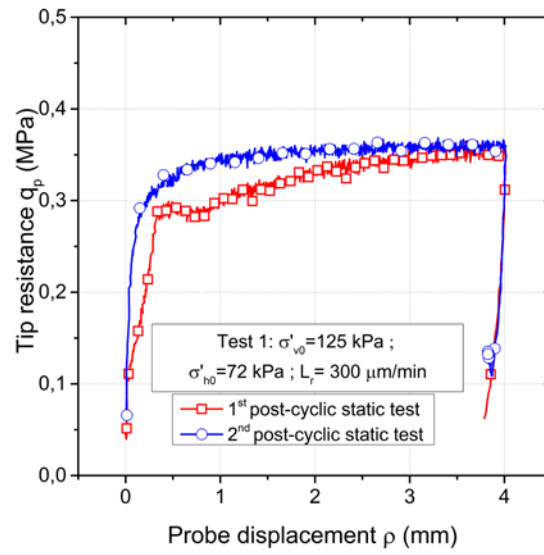


(a)

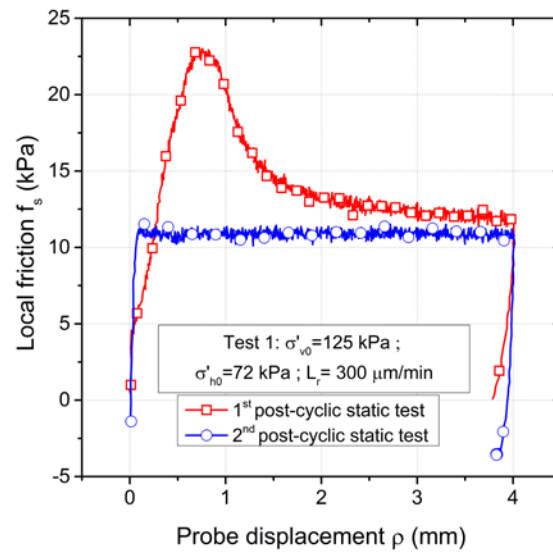


(b)

Fig. 12. Representation of selected cycles of friction mobilization for the typical test presented: (a) corresponding to the cyclic degradation phase, (b) corresponding to the cyclic reinforcement phase



(a)



(b)

Fig. 13. Final static loading phase: (a) tip resistance versus vertical displacement, (b) local friction versus vertical displacement

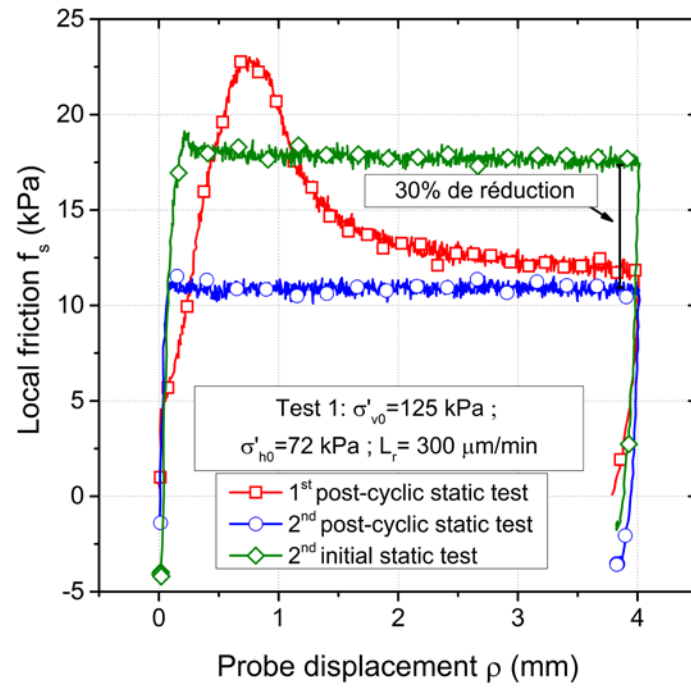


Fig. 14. Comparison between the initial and final static load tests in terms of local friction

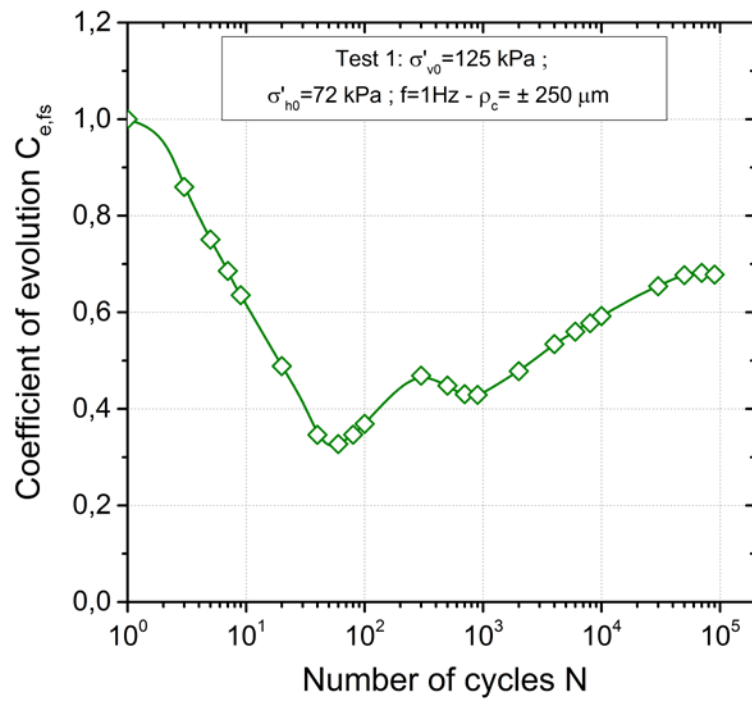


Fig. 15. Coefficient of evolution  $C_{e,fs}$  versus number of cycles for the test presented

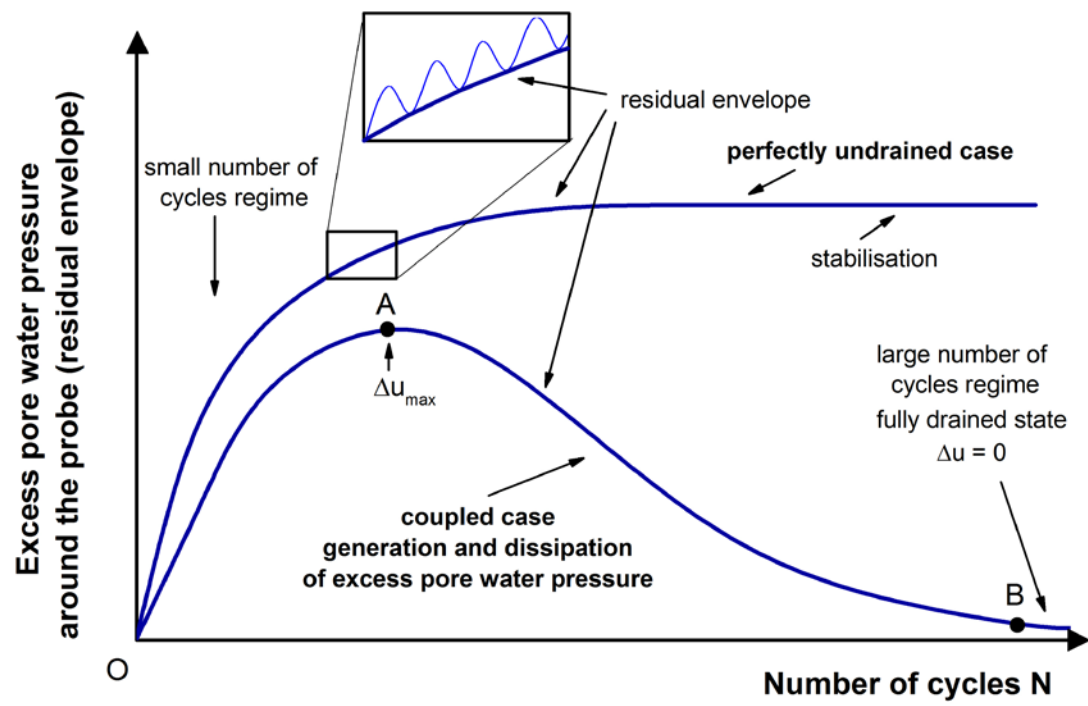


Fig. 16. Conceptual scheme of excess pore water pressure generation and dissipation around the pile-probe sleeve friction

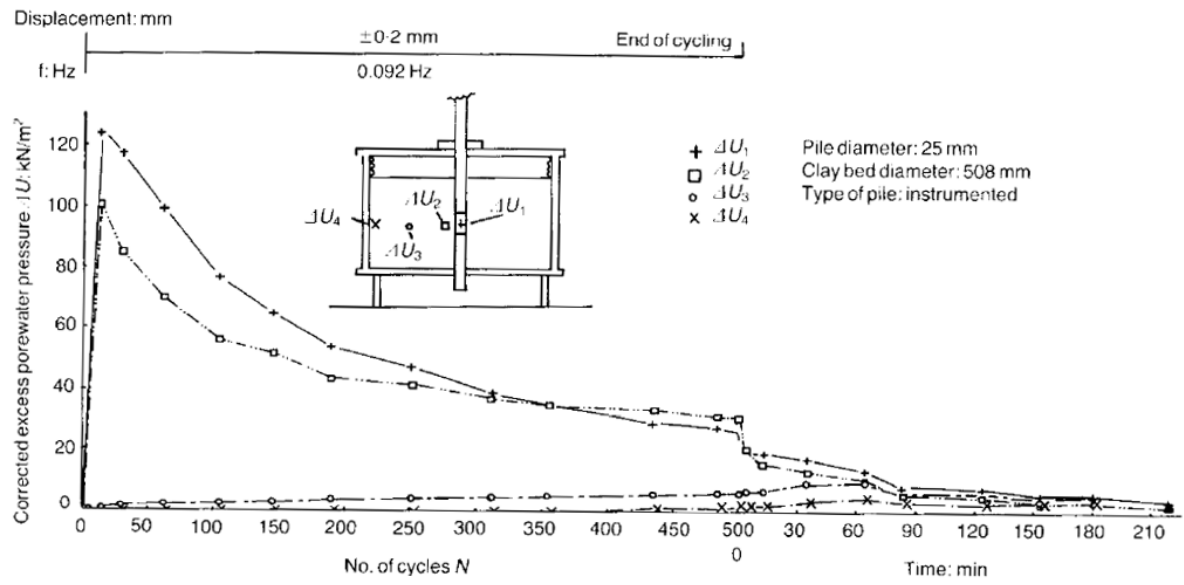


Fig. 17. Excess pore water pressure evolution during a displacement controlled cyclic test on a model pile element (Procter and Khaffaf, 1987)

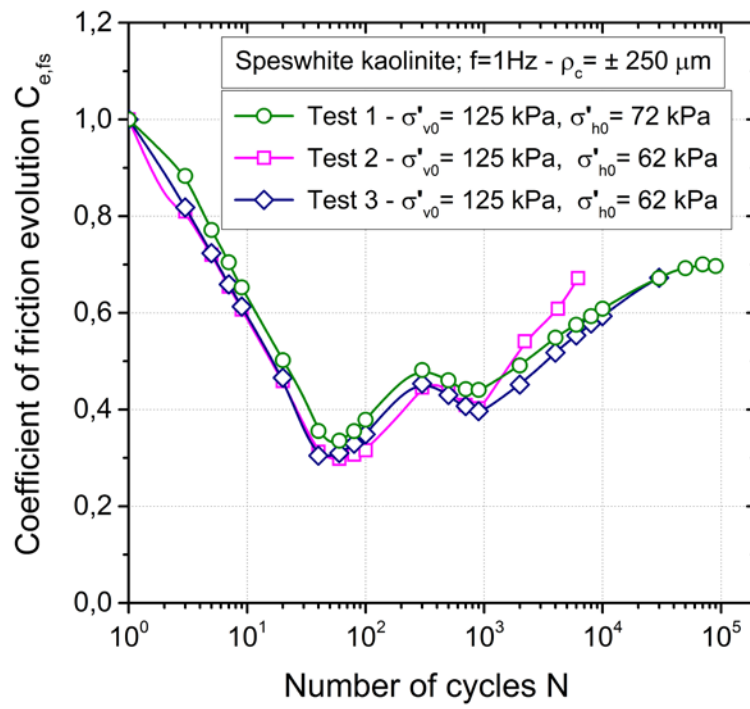


Fig. 18. Evaluation of test repeatability in terms of  $C_{e,fs}$  coefficient versus  
number of cycles

## Local soil-pile friction evaluation in saturated clays under cyclic loading

### TABLES

Mineralogy	Liquid Limit (%)	Plastic limit (%)	Plasticity index (%)	Soil particle density (t/m <sup>3</sup> )	Percent. finer than 10 $\mu\text{m}$ (%)
kaolinite	58	28	30	2,64	98

Table 1. Physical properties of Speswhite kaolinite

Test identification	$\sigma'_{v0}$ (kPa)	$\sigma'_{h0}$ (kPa)	Frequency $f$ (Hz)	$\rho_c$ ( $\mu\text{m}$ )	Number of cycles	Observations
Test 1	125	72	1	$\pm 250$	100 000	Reference test
Test 2	125	62	1	$\pm 250$	7 000	Repeatability test
Test 3	125	62	1	$\pm 250$	100 000	Repeatability test

Table 2. Main characteristics of tests performed